Published in final edited form as:

Phys Med. 2020 January ; 69: 19–27. doi:10.1016/j.ejmp.2019.11.021.

Beam angle optimization using angular dependency of range variation assessed via water equivalent path length (WEPL) calculation for head and neck proton therapy

Jihun Kim[1,2], **Yang-Kyun Park**[3], **Gregory Sharp**[1], **Paul Busse**[1], **Brian Winey**[1]

[1]Department of Radiation Oncology, Massachusetts General Hospital and Harvard Medical School, Boston, MA 02114, USA

[2]Department of Radiation Oncology, Yonsei University College of Medicine, Seoul, South Korea

[3]Department of Radiation Oncology, The University of Texas Southwestern Medical Center, Dallas, TX 75390, USA

Abstract

Purpose—To investigate angular sensitivity of proton range variation due to anatomic change in patients and patient setup error via water equivalent path length (WEPL) calculations.

Methods—Proton range was estimated by calculating WEPL to the distal edge of target volume using planning CT (pCT) and weekly scatter-corrected cone-beam CT (CBCT) images of 11 head and neck patients. Range variation was estimated as the difference between the distal WEPLs calculated on pCT and scatter-corrected CBCT (cCBCT). This WEPL analysis was performed every five degrees ipsilaterally to the target. Statistics of the distal WEPL difference were calculated over the distal area to compare between different beam angles. Physician-defined contours were used for the WEPL calculation on both pCT and cCBCT, not considering local deformation of target volume. It was also tested if a couch kick (10°) can mitigate the range variation due to anatomic change and patient setup error.

Results—For most of the patients considered, median, 75% quantile, and 95% quantile of the distal WEPL difference were largest for posterior oblique angles, indicating a higher chance of overdosing normal tissues at distal edge with these angles. Using a couch kick resulted in decrease in the WEPL difference for some posterior oblique angles.

Conclusions—It was demonstrated that the WEPL change has angular dependency for the cohort of head and neck cancer patients. Selecting beam configuration robust to anatomic change in patient and patient setup error may improve the treatment outcome of head and neck proton therapy.

Corresponding Author: Brian Winey, winey.brian@mgh.harvard.edu, 55 Fruit St, Boston, MA 02114.

Keywords

water equivalent path length; angular dependency; proton therapy; anatomic change; patient setup error; cone-beam CT; scatter correction

1. Introduction

Treatment outcome of proton therapy can deteriorate due to geometric uncertainties, such as anatomic change in patients and patient setup error [1–3]. Many head and neck cancer patients undergo substantial weight loss over the course of radiation treatment, resulting in unexpectedly excessive irradiation to normal surrounding tissues [4,5]. Furthermore, there still remains a possibility of misalignment that may negatively affect treatment outcome even when six degrees-of-freedom couch correction is performed using daily treatment imaging modality such as CBCT. Dosimetric impact of patient setup uncertainty was reported in previous studies [6,7]. Although proton therapy has dosimetric advantage over photon radiotherapy [8–11], rapid fall-off at distal edge can make proton therapy more sensitive to geometric uncertainties.

Range uncertainties have been dealt in robust optimization in many previous studies: (1) patient setup error and (2) range calculation uncertainty due to stopping power conversion error [12–17]. In the previous studies, the optimized treatment plan resulted in better clinical outcomes under the existence of such range uncertainties, for instance, 3 mm of patient setup error and 3.5% of range uncertainty.

Finding proton beam configuration robust to geometric uncertainties should be an interesting research question in the area of robust optimization since it can further improve plan robustness compared to experience-based proton beam angle selection. In Cao *et al.* [18], a beam angle optimization was performed to find a robust beam angle configuration for intensity-modulated proton therapy (IMPT). As results, better organ sparing was achieved with all plans with optimized beam angles than those with conventionally chosen beam angles.

Optimal beam angle selection for proton therapy can be also achieved by estimating range variation via WEPL calculation [18,19]. Recently, Yu *et al.* investigated a feasibility of WEPL-based beam angle selection method for plan robust optimization of IMPT of esophageal cancers [19]. In this previous work, WEPL was calculated to estimate range variations due to respiratory and diaphragmatic motion during free breathing. The IMPT plan calculated with the beam configuration favored by the WEPL analysis was shown to be also dosimetrically favorable, demonstrating the feasibility of the WEPL analysis to select proton beam angles robust to anatomic change in patient and patient setup error.

The purpose of this study is to investigate angular dependency of the range variation estimated via WEPL calculation due to anatomic change in patient and patient setup error during a course of head and neck proton therapy. To the best of authors' knowledge, this is first to use scatter-corrected CBCT images to assess the angular sensitivity of the longitudinal range variation due to anatomic change in head and neck patients. Advanced understanding of the angular dependency of the range variation may result in better selection of proton beam angles, thus improve treatment quality under the existence of the geometric uncertainties.

2. Material and Methods

2.1. Data acquisition

Eleven head and neck cancer patients who received photon radiotherapy and weekly CBCT exams as well as a planning CT exam were considered for a retrospective study. Two patients out of 13 patients included in the previous study [20] were removed in this study. For the two patients eliminated, WEPL calculation was not feasible for some range of angles since the CBCT scans were incomplete due to field of view cropping of CBCT. For treatment planning, patients were initially examined using a large bore GE CT scanner with 140 kVp tube voltage, 0.6–1.1 mm pixel size, and 2.5 mm slice thickness. For patient positioning and weekly verification of setup, patients were re-scanned at treatment using an Elekta XVI system with 100 kVp tube voltage, 10 mA tube current, 10 ms exposure time, no bowtie filter, and small panel position (centered detector, full fan) with a 20 cm collimator. The patients were scanned on a weekly basis, but some patients were additionally scanned if necessary. The number of days elapsed after planning CT exam to each CBCT scan are summarized in Table 1.

Each reconstructed CBCT image was subject to the CBCT scatter correction process. Recent studies demonstrated the feasibility of calculating WEPL on CBCT via scatter correction either using deformable image registration [21–25] or using *a priori*-based algorithm [20,26–29]. In this study, an existing *a priori*-based CBCT scatter correction algorithm was utilized. The resulting scatter-corrected CBCT images were reconstructed into an image with a field of view of 400 × 400 mm^2 and a CT scan length of 200 mm; the voxel size was 1.0 mm for each direction (details of the CBCT scatter correction can be found in Kim *et al.* [20]). Each scatter-corrected CBCT image was aligned using a 6 degrees-of-freedom rigid transformation (translation/rotation) obtained by an automatic rigid registration using Plastimatch [30]. Finally, the scatter-corrected CBCT image aligned to pCT, which is denoted by cCBCT, represented the patient anatomy during radiation treatment.

2.2. Target volume definition

Physician-defined contours of target volume generated for treatment planning and rigidly aligned to the weekly CBCT images were utilized for the WEPL calculation on pCT and cCBCT images. Figure 1 shows a physician-defined tumor contour overlaid on axial cuts of (a) planning CT image and (b) scatter-corrected CBCT image (last available fraction) of patient 1. The tumor contour was relatively well aligned in the middle of the patient where less volumetric change occurs compared to peripheral regions. The rigidly-aligned contour near the patient's exterior shows volumetric loss during radiation treatment. Using rigidly aligned contours allows for the constant comparison of distal WEPL values across the entire treatment course and displays the effects of using a single treatment plan.

2.3. Distal WEPL difference

Distal edges were detected from the target contours and WEPL was calculated to the resulting distal edges (distal WEPL) using an in-house software. The proton range variation due to anatomic change and patient setup error was evaluated by calculating variation in the distal WEPL, ΔWEPL. To calculate ΔWEPL, WEPLs were calculated to the distal edges of target volume with baseline pCT and weekly cCBCT. Equation (1) describes the mathematical definition of ΔWEPL:

$$\Delta WEPL = WEPL_{pCT} - WEPL_{cCBCT} \quad (1)$$

where $WEPL_{pCT}$ and $WEPL_{cCBCT}$ represent WEPL calculated using pCT and cCBCT, respectively.

When using a rigidly-aligned target, the inclusion of voxels outside the patient can affect the distal WEPL variation calculation of Equation 1 but only for small regions of the distal surface for beams with a limited angular range parallel to the skin surface. This is because the changes in the skin surface displayed in Figure 1 would be in the proximal region for most beam directions. To evaluate the effects of the using rigidly-aligned targets that might include some distal points outside the patient, the distal WEPL analysis was repeated after elimination of all voxels outside the patient surface for Patient 1 which displayed the largest anatomic changes.

2.4. Angular ΔWEPL calculation

In order to see if the range variation due to anatomic change and patient setup error has angular dependency, ΔWEPL was calculated for proton beam angles between 0° and 180° with an interval of 5° when the target volume was located on the left side of the patient (angles between 180–360 ° were used for the target volume on the right side); the angles were represented following the standards provided by the International Electrotechnical Commission (IEC 61217). In Table 1, it was summarized on which side of the neck the target volume considered for the WEPL calculation was located. This WEPL difference calculation was performed for each of the weekly CBCT scans to see its time dependency as well as angular dependency. Statistics of the distal WEPL difference were calculated to compare for the proton beam angles considered: median and quantiles (5%, 25%, 75%, and 95%).

Moreover, the impact of couch kick on the WEPL variation was investigated. Specifically, it was tested if using a couch kick can reduce the range variations geometrically amplified as proton beams pass through trapezius muscle in the patient shoulder. The rationale behind this test is that small geometric change in the shoulder can result in large range variations; the muscle exterior is nearly parallel to the proton beams without couch kick. Superior oblique beam angles were simulated by rotating both pCT and cCBCT images by 10° for the patients having the target volume on the right side (by −10° for the others). This couch kick test was performed for three patients (patients 1, 2, and 8), for which some shoulder region was included within the CBCT FOV.

It was investigated how much the statistics of WEPL difference were influenced if the points outside the patient were removed. A few points in the distal edge of the target volume were located outside the patient geometry at treatment due to volumetric loss. The WEPL differences calculated at these off-patient points may not be clinically relevant in case that the corresponding proton rays do not pass through anywhere in the patient.

3. Results

3.1. Angular variation of distal WEPL

Figure 2 shows the beam's eye view (BEV) distal WEPL difference maps calculated with two different proton beam angles, anterior oblique (45°) and posterior oblique (135°) for patient 1. Some aspects of angular dependency can be seen in the comparison of the BEV WEPL difference maps in Fig. 2. WEPL differences over all distal area were larger for the posterior oblique beam than for the anterior oblique beam: 6.6 ± 2.8 mm vs. 9.2 ± 7.0 mm. These results demonstrated that the same volumetric change (seen in Fig. 1) resulted in different WEPL differences depending on the proton beam direction. It is noted that the WEPL calculation uncertainty using scatter-corrected CBCT (2% of WEPL demonstrated in Park *et al.* [28]) was found to be relatively small compared to the resulting WEPL differences.

Figure 3 shows both temporal and angular variations of the distal WEPL difference for patient 1. Median and four different quantiles (5%, 25%, 75%, and 95%) of the distal WEPL difference were displayed in box plots for 2^{nd} (black), 4^{th} (dark gray), and 6^{th} (light gray) weeks. For all the beam angles considered, the distal WEPL difference increased with the number of treatment fractions that the patient underwent. As can be seen in Fig. 3, the WEPL calculation results show that overdosing normal tissues at distal edge is more likely to occur than underdosing the target volume. With anterior and posterior beams, insufficient radiation dose can be delivered to some of the target volume for this patient, possibly due to patient setup error. The median values of the WEPL differences were between 0 and 10 mm for all the beam angles. Large distal WEPL differences were most found with posterior oblique angles for this patient, i.e. 120–150°.

Details of the distal WEPL difference calculated for the last weekly fraction of patient 1 can be further explored in Figure 4, supplementing Figure 3. Percentages of the distal WEPL difference for different ranges were displayed in a stacked bar graph. Different characteristics of the range variation can be seen for the beam angles considered. First, with anterior and posterior angles, both overshooting and undershooting are expected. It is noted that, however, with posterior angle the highest percentage was obtained for $-5 \leq \Delta\text{WEPL} < 5$ mm. Second, for the angles between 60 and 100°, the percentage of undershooting ($\Delta\text{WEPL} < 0$ mm) was less than 1%. In addition, for these angles (60–100°), the percentage of the distal WEPL differences over 10 mm was relatively small. Some posterior oblique angles (120–150°) showed higher percentages of such large WEPL differences. For instance, the maximum percentage of $\Delta\text{WEPL} \geq 10$ mm was found to be 40% at the angle of 135°.

Figure 5 shows angular variation of WEPL difference for all patients. Similar angular dependency of distal WEPL difference seen in Fig. 3 was also seen in Fig. 5, demonstrating that a common angular dependency can be observed in majority of the patient cohort considered. Using anterior and posterior beam angles (0° and 180°) may have higher chances of both underdosing target volume and overdose normal tissues at distal edge compared to lateral beam angles (60–100°). In general, posterior oblique angles (120–160°) and anterior angle (0°) were most sensitive to anatomic change and patient setup error in terms of overdosing normal tissue. For all the beam angles taken into consideration, most of the WEPL differences were found to be between 0 and 10 mm. Maximum overshooting (95% quantile) was within 15 mm and median value of WEPL difference was within 5 mm for all the beam angles. Table 2 summarizes the statistics (median, 95% quantile, and 5% quantile) of the distal WEPL differences calculated for various beam angles (0°, 20°, 40°, 60°, 80°, 100°, 120°, 140°, 160°, and 180°) for all patients. Considering all the statistical metrics, lateral beams of 60–100° were found to be optimal to minimize the range variations due to anatomic change in patient and patient setup error. On the other hand, the range variation was relatively large for anterior beam (0°) and posterior beam angles of 120–160°.

3.2. Impact of couch kick

Figure 6 shows BEV WEPL differences calculated for a posterior oblique angle (135°) without and with a couch kick for patients 1, 2, and 8. The WEPL differences shown in Fig. 6 were calculated using pCT and last weekly CBCT image. For all three patients considered, the WEPL differences were large at the bottom of the BEV WEPL difference maps, which were caused by geometric or positional change of trapezius muscle in the shoulder region. However, these large WEPL differences were reduced by applying a couch kick of 10°. It should be noted that, for patient 1, the mean WEPL difference increased from 9.2 mm in Fig. 6 (a) to 9.4 mm in Fig. 6 (b). This increase is attributed to the large WEPL differences at the top (see inside a dashed circle in Fig. 6 (b)) due to positional uncertainty of the patient ear. The proton beam with the couch kick passed through more of the patient ear than without the couch kick.

Figure 7 shows the impact of a couch kick on the distal WEPL difference for various angles (patient 8). A noticeable decrease of median, 75% quantile, and 95% quantile was found for some posterior oblique angles (125–150°), shown enclosed by dashed lines. This finding demonstrated that the use of a couch kick (10°) lead to an improvement in regard of relatively large range variation due to anatomic change and/or positional error for a range of beam angles between 125° and 150° although average range variation was slightly reduced.

3.3. Off-patient points in distal edge

Figure 8 shows the comparison of the BEV WEPL difference maps calculated for a beam angle of 150° for patient 1: with vs. without off-patient points. The beam angle chosen for the BEV comparison in Fig. 8 was one of the angles for which the results were most affected by removing the off-patient points (see Figure 9). For this beam angle, 183 points out of 3586 were removed (5.1%). As a consequence, large WEPL differences were eliminated, resulting in decrease in the WEPL differences: 8.8 ± 8.7 (mm) to 7.6 ± 6.8 (mm)

A comparison of box plots of the WEPL differences calculated for various beam angles was made in Fig. 9. By eliminating off-patient points, the WEPL differences were most affected for some posterior oblique angles. As can be seen from Fig. 9, 95% quantiles were noticeably reduced for posterior oblique angles between 140° and 160°. However, the overall trend did not change after excluding off-patient points.

4. Discussion

The distal WEPL variation due to anatomic change in patient and patient setup error has a similar angular dependency for the cohort of 11 head and neck cancer patients. Specifically, posterior oblique angles between 120° and 160° were most sensitive to the geometric uncertainties. This angular dependency was seen because volumetric change (in general, volume loss) occurred in head and neck patients was geometrically amplified from these angles as illustrated in Fig. 2. Although most of head and neck patients have similar geometry and directivity of volumetric loss, a different angular dependency may be seen for some patients having a different geometry. In addition, inconsistent patient setup may have influence on the angular dependency of the WEPL difference.

It was demonstrated that relatively large range variation in patient occurred due to anatomic change with some posterior oblique angles. As shown in Fig. 1, the WEPL differences calculated with posterior oblique angles can include some large values calculated at a few off-patient distal points due to lack of consideration of local deformation. Since these large WEPL differences do not implicate overshooting during treatment, the impact of anatomic change in patient could be overestimated. However, largest WEPL decreases were calculated at the points near the patient skin and inside the patient geometry, indicating a possibility of large overshoots beyond the distal edge. For the head and neck patients considered, the distal WEPL decreased on average over all beam angles, indicating that the impact of volume loss was dominant over that of patient setup uncertainty. A different tendency of WEPL change can be observed for patients with other tumor types/locations.

Using physician-defined contours without any consideration of local deformation to calculate WEPLs on both pCT and cCBCT may introduce a source of uncertainty into the calculated WEPL differences and, therefore, into the angular dependency. However, as previously discussed, relatively small deformations may occur at the distal edge. Moreover, it is a challenging task to define target volume on each treatment day. Manual contouring by radiation oncologist on each weekly treatment scan is time-consuming and practically not feasible. An alternative way to define treatment target volume is to adapt the target volume using deformable image registration. It should be noted that this method can introduce another source of uncertainty due to inevitable registration errors [31,32].

For head and neck cancer patients, three proton fields from three different beam directions are frequently used. Two common beam angle configurations are (1) left and right anterior oblique angles and a single posterior angle (Y-shaped configuration), and (2) left and right posterior oblique angles and a single anterior angle (inverted Y-shaped configuration). The results of the WEPL analysis demonstrated that Y-shaped configuration is more robust to anatomic change and patient setup error than inverted Y-shaped configuration, although the inverted Y shaped configuration might provide a more preferable dose distribution

It is noted that the distal WEPL difference was calculated to estimate the extent of underdosing of target volume and overdosing of normal tissues. Any changes in dose distribution have not been considered in this study. Recent studies reported correlations between WEPL-based measure and dosimetric change [19,24,25,33]. Such a correlation and actual dosimetric impact on organs-at-risk, which is out of scope of this study, will be investigated for head and neck proton therapy in a future study.

Using a couch kick with some posterior oblique angles can mitigate the range variation due to anatomic change and patient setup error in the inferior portion of the treatment fields where the shoulders can introduce patient setup challenges. The mitigating impact of the couch kick can be larger than shown in this study because some of the inferior part of the target volume was cropped in the CBCT images and not included in the WEPL calculations. It should be noted that, however, the use of the couch kick may result in increased range errors at the top of the field when the target volume is located up to the level of the patient ear and the proton beams pass through the patient ear.

5. Conclusions

Angular dependency was observed in the proton range variation over the course of treating head and neck patients estimated by calculating distal WEPL differences on cCBCT images. Posterior oblique proton beam angles were most sensitive to anatomic change and patient setup error for most of the cohort of 11 head and neck patients, although the WEPL variations for posterior oblique beams were reduced with couch kicks. This finding suggests the preference for treatment angles other than posterior obliques and posterior oblique angle combined with a couch kick to mitigate the range variation due to anatomic changes and patient setup uncertainty.

Acknowledgments

This work was supported by the NCI Federal Share of program income earned by Massachusetts General Hospital on C06 CA059267, Proton Therapy Research and Treatment Center.

References

[1]. Lomax AJ. Intensity modulated proton therapy and its sensitivity to treatment uncertainties 1: the potential effects of calculational uncertainties. Phys Med Biol 2008;53:1027–42. doi: 10.1088/0031-9155/53/4/014. [PubMed: 18263956]

[2]. Lomax AJ. Intensity modulated proton therapy and its sensitivity to treatment uncertainties 2: the potential effects of inter-fraction and inter-field motions. Phys Med Biol 2008;53:1043–56. doi: 10.1088/0031-9155/53/4/015. [PubMed: 18263957]

[3]. Kraan AC, van de Water S, Teguh DN, Al-Mamgani A, Madden T, Kooy HM, et al. Dose uncertainties in IMPT for oropharyngeal cancer in the presence of anatomical, range, and setup errors. Int J Radiat Oncol Biol Phys 2013;87:888–96. doi:10.1016/j.ijrobp.2013.09.014. [PubMed: 24351409]

[4]. Lee C, Langen KM, Lu W, Haimerl J, Schnarr E, Ruchala KJ, et al. Evaluation of geometric changes of parotid glands during head and neck cancer radiotherapy using daily MVCT and automatic deformable registration. Radiother Oncol 2008;89:81–8. doi:10.1016/j.radonc.2008.07.006. [PubMed: 18707786]

[5]. Lee C, Langen KM, Lu W, Haimerl J, Schnarr E, Ruchala KJ, et al. Assessment of parotid gland dose changes during head and neck cancer radiotherapy using daily megavoltage computed

tomography and deformable image registration. Int J Radiat Oncol Biol Phys 2008;71:1563–71. doi:10.1016/j.ijrobp.2008.04.013. [PubMed: 18538505]

[6]. Hong TS, Tomé WA, Chappell RJ, Chinnaiyan P, Mehta MP, Harari PM. The impact of daily setup variations on head-and-neck intensity-modulated radiation therapy. Int J Radiat Oncol Biol Phys 2005;61:779–88. doi:10.1016/j.ijrobp.2004.07.696. [PubMed: 15708257]

[7]. Siebers J V, Keall PJ, Wu Q, Williamson JF, Schmidt-Ullrich RK. Effect of patient setup errors on simultaneously integrated boost head and neck IMRT treatment plans. Int J Radiat Oncol Biol Phys 2005;63:422–33. doi:10.1016/j.ijrobp.2005.02.029. [PubMed: 16168835]

[8]. Steneker M, Lomax A, Schneider U. Intensity modulated photon and proton therapy for the treatment of head and neck tumors. Radiother Oncol 2006;80:263–7. doi:10.1016/j.radonc.2006.07.025. [PubMed: 16916557]

[9]. van de Water TA, Lomax AJ, Bijl HP, de Jong ME, Schilstra C, Hug EB, et al. Potential benefits of scanned intensity-modulated proton therapy versus advanced photon therapy with regard to sparing of the salivary glands in oropharyngeal cancer. Int J Radiat Oncol Biol Phys 2011;79:1216–24. doi:10.1016/j.ijrobp.2010.05.012. [PubMed: 20732761]

[10]. Kandula S, Zhu X, Garden AS, Gillin M, Rosenthal DI, Ang K-K, et al. Spot-scanning beam proton therapy vs intensity-modulated radiation therapy for ipsilateral head and neck malignancies: A treatment planning comparison. Med Dosim 2013;38:390–4. doi:10.1016/j.meddos.2013.05.001. [PubMed: 23916884]

[11]. Holliday EB, Garden AS, Rosenthal DI, Fuller CD, Morrison WH, Gunn GB, et al. Proton therapy reduces treatment-related toxicities for patients with nasopharyngeal cancer: a case-match control study of intensity-modulated proton therapy and intensity-modulated photon therapy. Int J Part Ther 2015;2:19–28. doi:10.14338/IJPT-15-00011.1.

[12]. Unkelbach J, Chan TCY, Bortfeld T. Accounting for range uncertainties in the optimization of intensity modulated proton therapy. Phys Med Biol 2007;52:2755–73. doi:10.1088/0031-9155/52/10/009. [PubMed: 17473350]

[13]. Unkelbach J, Bortfeld T, Martin BC, Soukup M. Reducing the sensitivity of IMPT treatment plans to setup errors and range uncertainties via probabilistic treatment planning. Med Phys 2009;36:149–63. doi:10.1118/1.3021139. [PubMed: 19235384]

[14]. Fredriksson A, Forsgren A, Hårdemark B. Minimax optimization for handling range and setup uncertainties in proton therapy. Med Phys 2011;38:1672–84. doi:10.1118/1.3556559. [PubMed: 21520880]

[15]. Liu W, Zhang X, Li Y, Mohan R. Robust optimization of intensity modulated proton therapy. Med Phys 2012;39:1079–91. doi:10.1118/1.3679340. [PubMed: 22320818]

[16]. Liu W, Frank SJ, Li X, Li Y, Park PC, Dong L, et al. Effectiveness of robust optimization in intensity-modulated proton therapy planning for head and neck cancers. Med Phys 2013;40:51711. doi:10.1118/1.4801899.

[17]. Frank SJ, Cox JD, Gillin M, Mohan R, Garden AS, Rosenthal DI, et al. Multifield optimization intensity modulated proton therapy for head and neck tumors: a translation to practice. Int J Radiat Oncol Biol Phys 2014;89:846–53. doi:10.1016/j.ijrobp.2014.04.019. [PubMed: 24867532]

[18]. Cao W, Lim GJ, Lee A, Li Y, Liu W, Zhu XR, et al. Uncertainty incorporated beam angle optimization for IMPT treatment planning. Med Phys 2012;39:5248–56. doi:10.1118/1.4737870. [PubMed: 22894449]

[19]. Yu J, Zhang X, Liao L, Li H, Zhu R, Park PC, et al. Motion-robust intensity-modulated proton therapy for distal esophageal cancer. Med Phys 2016;43:1111–8. doi:10.1118/1.4940789. [PubMed: 26936698]

[20]. Kim J, Park Y-K, Sharp G, Busse P, Winey B. Water equivalent path length calculations using scatter-corrected head and neck CBCT images to evaluate patients for adaptive proton therapy. Phys Med Biol 2017;62. doi:10.1088/1361-6560/62/1/59.

[21]. Kurz C, Dedes G, Resch A, Reiner M, Ganswindt U, Nijhuis R, et al. Comparing cone-beam CT intensity correction methods for dose recalculation in adaptive intensity-modulated photon and proton therapy for head and neck cancer. Acta Oncol (Madr) 2015;54:1651–7. doi:10.3109/0284186X.2015.1061206.

[22]. Landry G, Nijhuis R, Dedes G, Handrack J, Thieke C, Janssens G, et al. Investigating CT to CBCT image registration for head and neck proton therapy as a tool for daily dose recalculation. Med Phys 2015;42:1354–66. doi:10.1118/1.4-908223. [PubMed: 25735290]

[23]. Veiga C, Alshaikhi J, Amos R, Lourenço AM, Modat M, Ourselin S, et al. Cone-beam computed tomography and deformable registration-based “dose of the day” calculations for adaptive proton therapy. Int J Part Ther 2015;2:404–14. doi:10.14338/IJPT-14-00024.1.

[24]. Veiga C, Janssens G, Teng C-L, Baudier T, Hotoiu L, McClelland JR, et al. First clinical investigation of cone beam computed tomography and deformable registration for adaptive proton therapy for lung cancer. Int J Radiat Oncol Biol Phys 2016;95:549–59. doi:10.1016/j.ijrobp.2016.01.055. [PubMed: 27084664]

[25]. Wang P, Yin L, Zhang Y, Kirk M, Song G, Ahn PH, et al. Quantitative assessment of anatomical change using a virtual proton depth radiograph for adaptive head and neck proton therapy. J Appl Clin Med Phys 2016;17:427–40. doi:10.1120/jacmp.v17i2.5819. [PubMed: 27074464]

[26]. Niu T, Sun M, Star-Lack J, Gao H, Fan Q, Zhu L. Shading correction for on-board cone-beam CT in radiation therapy using planning MDCT images. Med Phys 2010;37:5395–406. doi:10.1118/1.3483260. [PubMed: 21089775]

[27]. Niu T, Al-Basheer A, Zhu L. Quantitative cone-beam CT imaging in radiation therapy using planning CT as a prior: First patient studies. Med Phys 2012;39:1991–2000. doi:10.1118/1.3693050. [PubMed: 22482620]

[28]. Park Y-K, Sharp GC, Phillips J, Winey BA. Proton dose calculation on scatter-corrected CBCT image: Feasibility study for adaptive proton therapy. Med Phys 2015;42:4449–59. doi:10.1118/1.4923179. [PubMed: 26233175]

[29]. Kurz C, Kamp F, Park Y-K, Zöllner C, Rit S, Hansen D, et al. Investigating deformable image registration and scatter correction for CBCT-based dose calculation in adaptive IMPT. Med Phys 2016;43:5635–46. doi:10.1118/1.4962933. [PubMed: 27782706]

[30]. Shackleford JA, Kandasamy N, Sharp GC. On developing B-spline registration algorithms for multi-core processors. Phys Med Biol 2010;55:6329–51. doi:10.1088/0031-9155/55/21/001. [PubMed: 20938071]

[31]. van Kranen S, Mencarelli A, van Beek S, Rasch C, van Herk M, Sonke J-J. Adaptive radiotherapy with an average anatomy model: evaluation and quantification of residual deformations in head and neck cancer patients. Radiother Oncol 2013;109:463–8. doi:10.1016/j.radonc.2013.08.007. [PubMed: 24021348]

[32]. Mencarelli A, van Kranen SR, Hamming-Vrieze O, van Beek S, Nico Rasch CR, van Herk M, et al. Deformable image registration for adaptive radiation therapy of head and neck Cancer: accuracy and precision in the presence of tumor changes. Int J Radiat Oncol Biol Phys 2014;90:680–7. doi:10.1016/j.ijrobp.2014.06.045. [PubMed: 25151537]

[33]. Matney JE, Park PC, Li H, Court LE, Zhu XR, Dong L, et al. Perturbation of water-equivalent thickness as a surrogate for respiratory motion in proton therapy. J Appl Clin Med Phys 2016;17:368–78. doi:10.1120/jacmp.v17i2.5795. [PubMed: 27074459]

Highlights

- For posterior oblique angles, proton range variation is most sensitive to anatomic change in patients and patient setup error.
- Angular dependency of proton range variation was observed in 11 head and neck patients.
- Dosimetric impact of proton range variation may be reduced by selecting an optimal beam configuration.
- Calculating WEPL on scatter-corrected CBCT is a viable option to evaluate proton range variation.

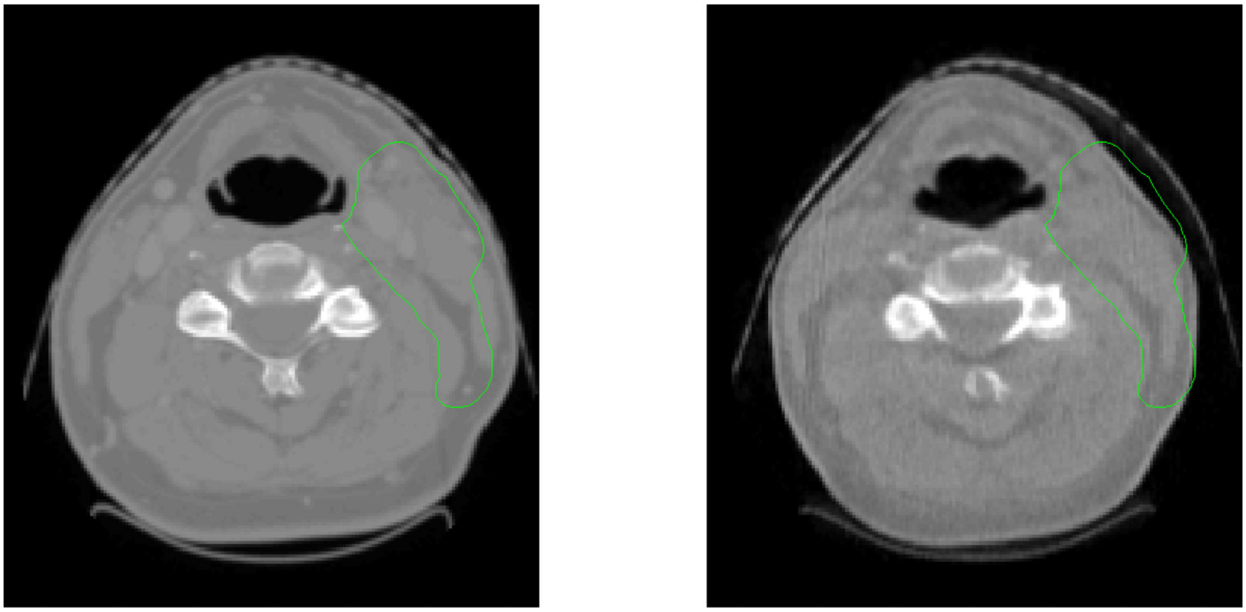

(a)
(b)

Figure 1.
Overlay of a physician-defined tumor contour on an axial cut of (a) a planning CT image and (b) a scatter-corrected CBCT image.

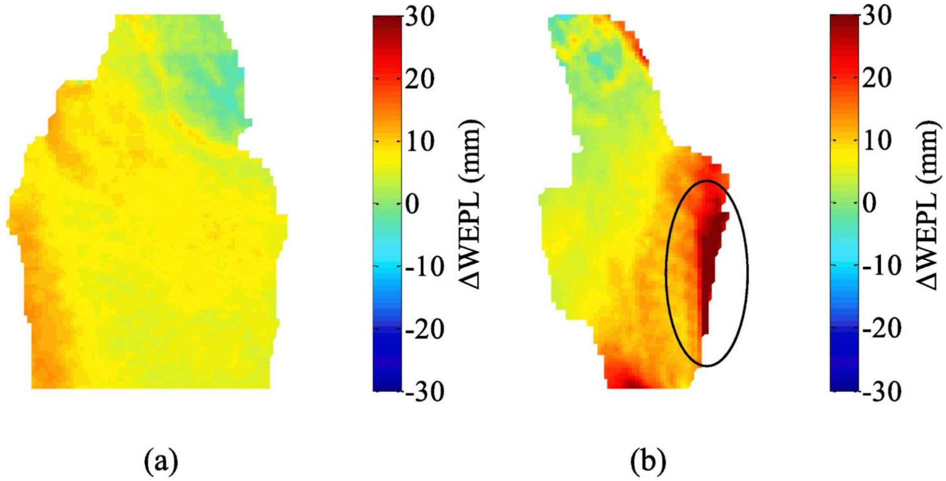

Figure 2.
Beam's eye view WEPL difference maps calculated for the last available CBCT scan for patient 1 with the beam angles of (a) 45° and (b) 135°. Note that some of the excessive range variations inside the circle were calculated at the points outside the patient.

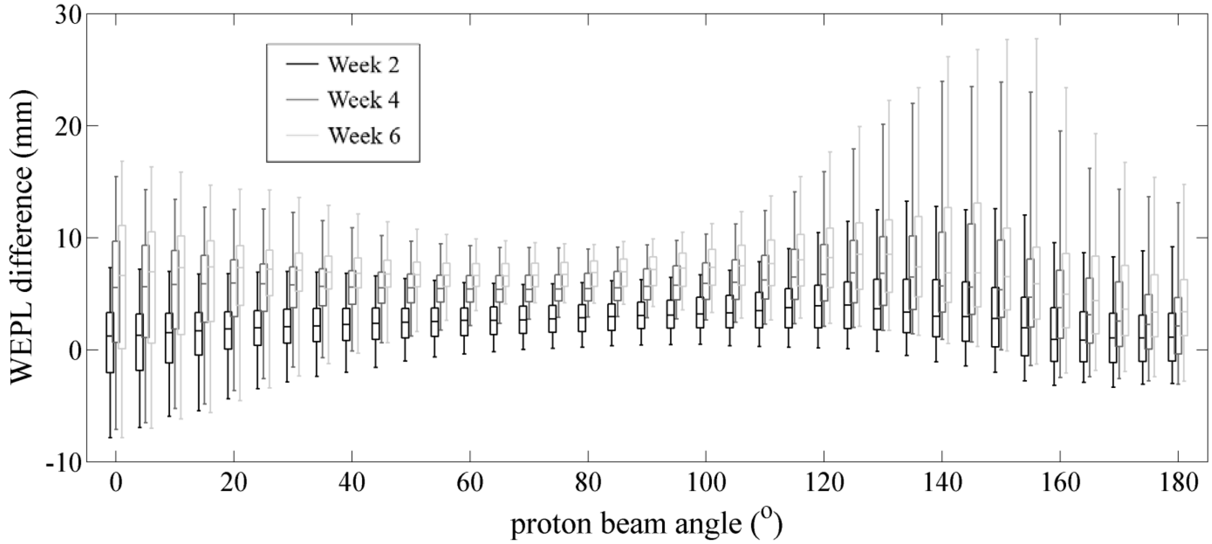

Figure 3.
Box plots of median and quantiles (5%, 25%, 75%, and 95%) of distal WEPL difference for 2nd (black), 4th (dark gray), and 6th (light gray) weeks for patient 1.

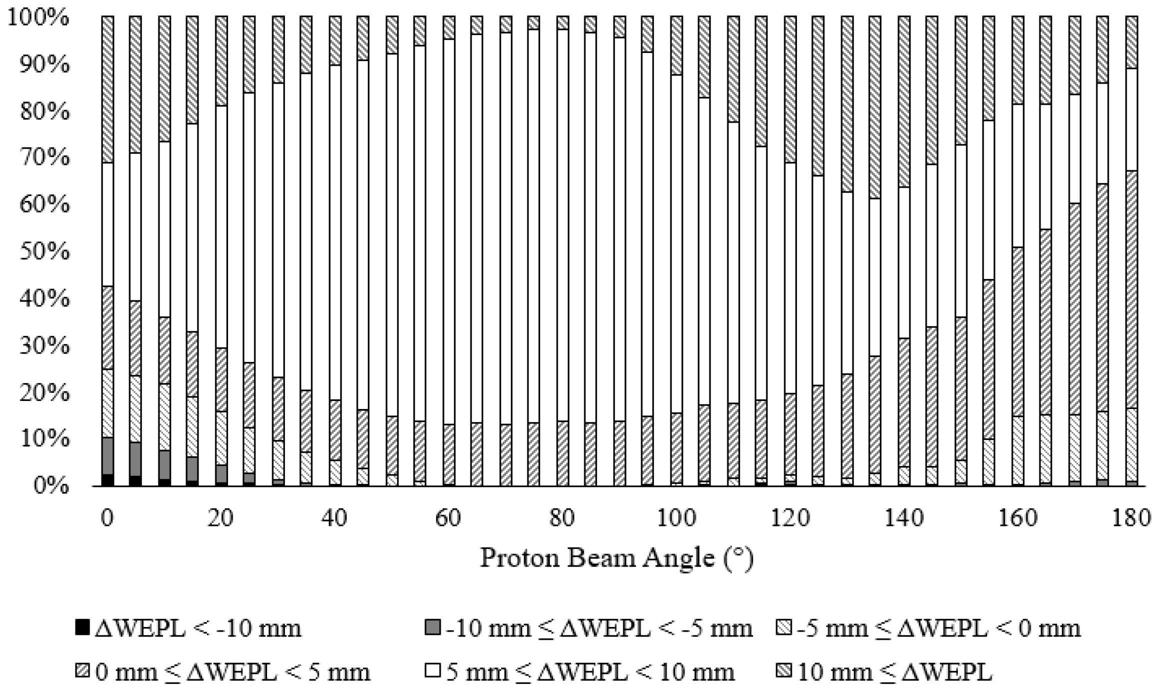

Figure 4.

Stacked bar graph of percentages of distal WEPL differences for the last weekly fraction of patient 1.

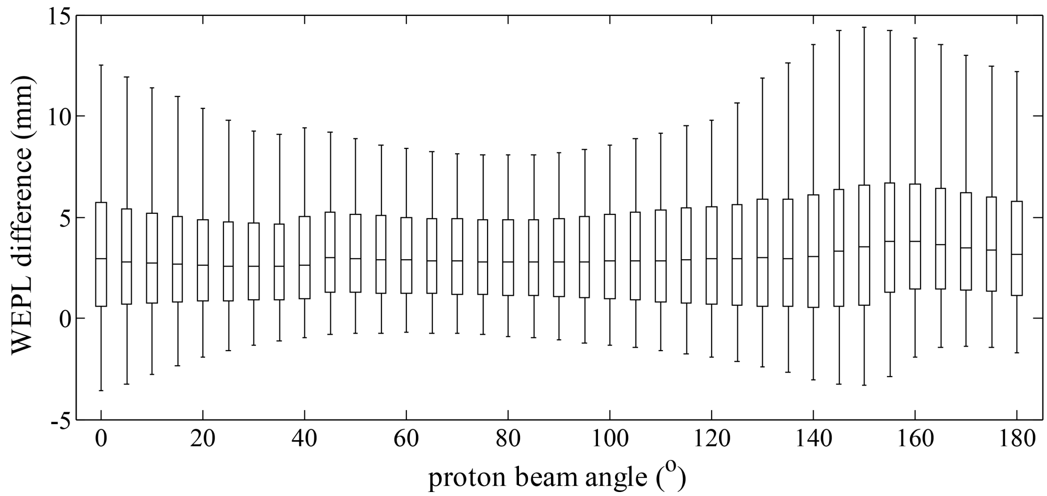

Figure 5.
Box plots of median and quantiles (5%, 25%, 75%, and 95%) of distal WEPL difference for all weeks of all patients.

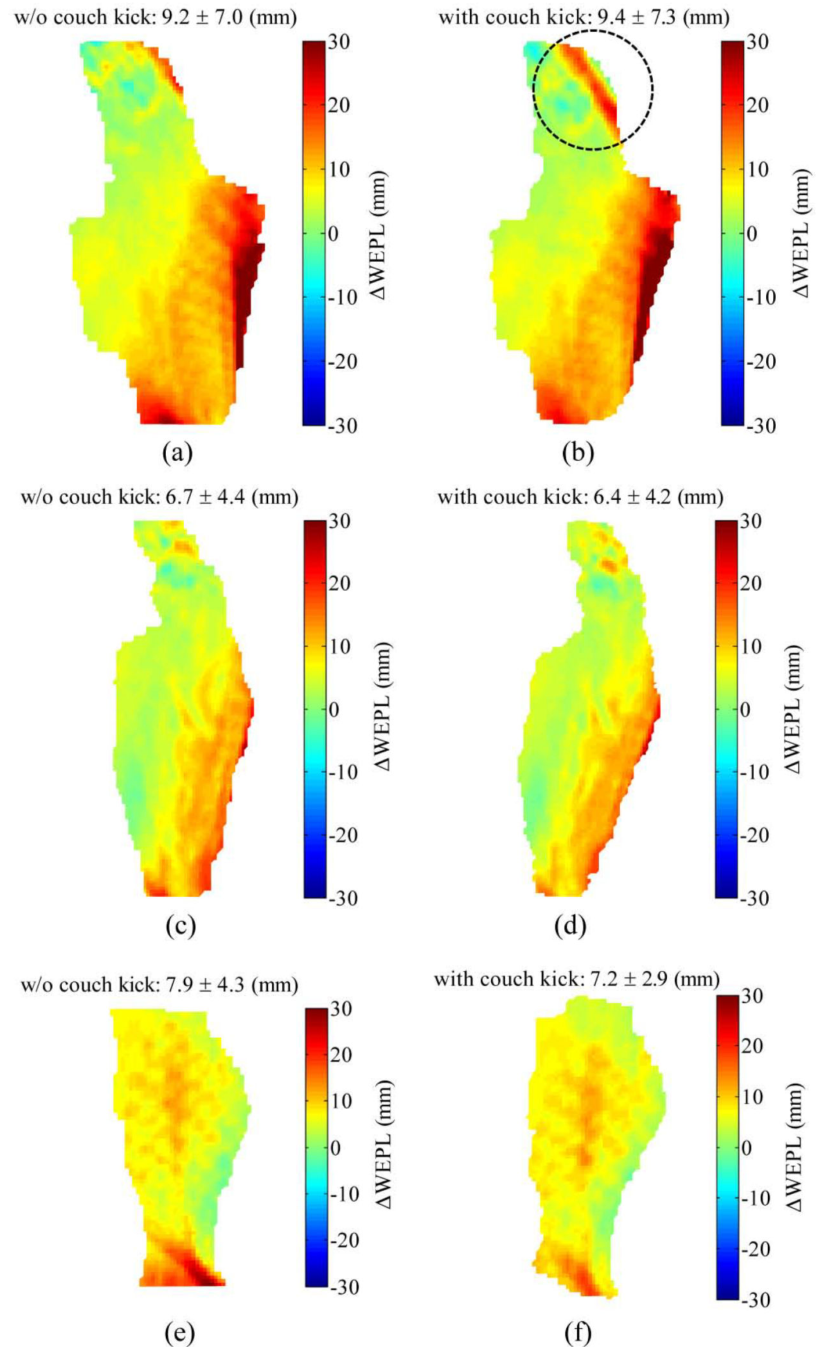

Figure 6.

Comparisons of last week's BEV WEPL difference maps calculated for a posterior-oblique angle (135°): without couch kick (left column) vs. with couch kick (right column) for patients 1 ((a), (b)), 2 ((c), (d)), and 8 ((e), (f)). Mean ± standard deviation of the WEPL differences are also presented. Large WEPL difference in a dashed circle was due to positional uncertainty of the patient ear.

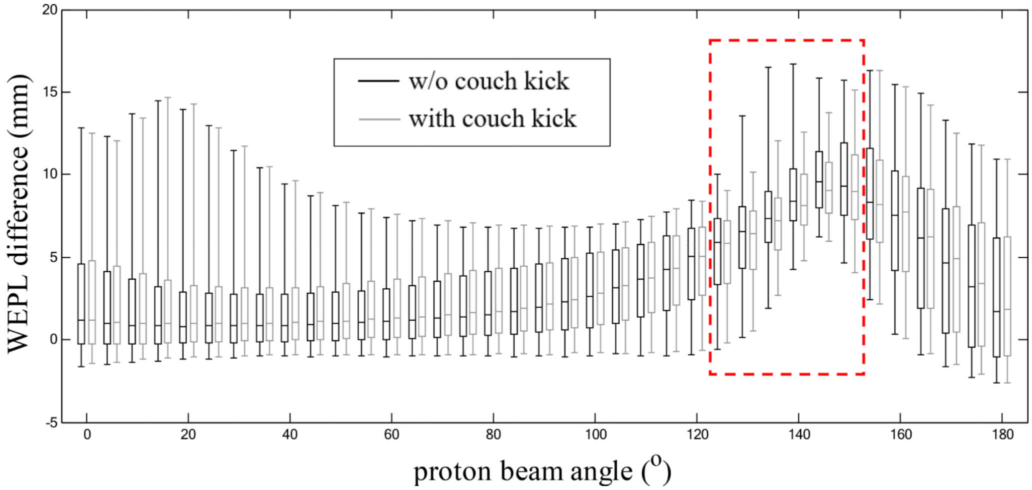

Figure 7.

Box plots of median and quantiles (5%, 25%, 75%, and 95%) of distal WEPL differences calculated without and with a couch kick for patient 8.

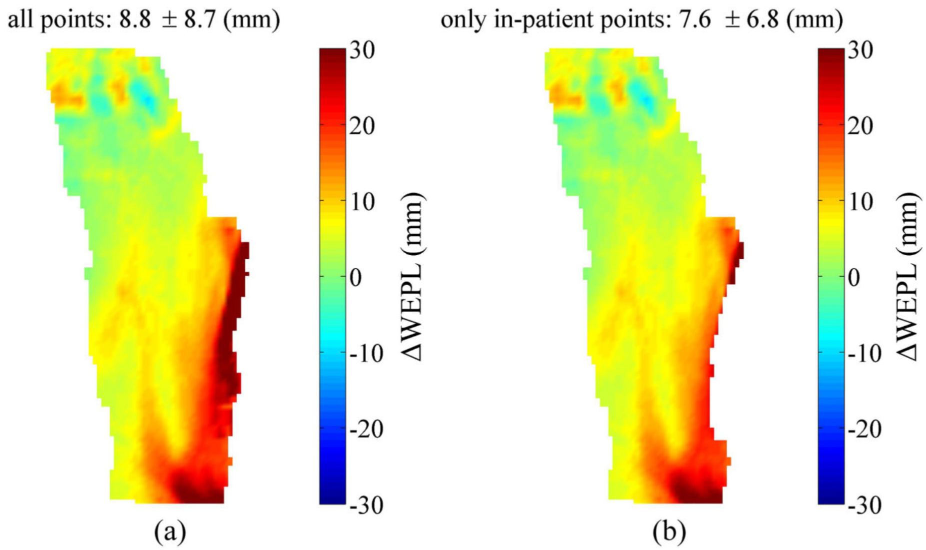

Figure 8.

Comparisons of last week's BEV WEPL difference maps calculated for a beam angle (150°): (a) including vs. (b) excluding off-patient points for patients 1. Mean ± standard deviation of the WEPL differences are presented.

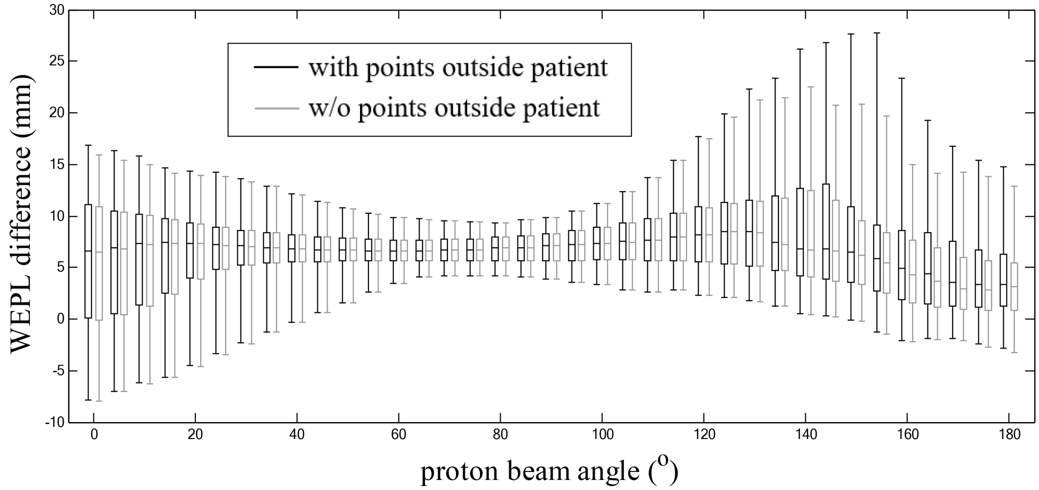

Figure 9.

Box plots of median and quantiles (5%, 25%, 75%, and 95%) of distal WEPL differences calculated with and without off-patient points for patient 1.

Table 1.

For each patient, list of acquired CBCTs with the number of days elapsed since the pCT simulation and location of the PTV

		Elapsed days after pCT simulation						
Patient no.	**PTV location**	**1**	**2**	**3**	**4**	**5**	**6**	**7**
1	left	22	29	36	37	43	50	
2	left	22	29	37	43	50	55	
3	left	15	23	30	37	44	51	58
4	right	21	28	35	42	49	56	63
5	left	34	35	42	49	59		
6	right	19	26	33	40	47	48	49
7	left	14	21	22	28	35	43	
8	left	14	21	22	23	29	36	
9	left	21	28	35	36	43		
10	left	14	21	28	35	42	50	
11	left	14	21	28	35	43	46	47

Table 2.

Statistics of the distal WEPL differences calculated using pCT and final weekly cCBCT for various beam angles for all patients: median, 95% quantile, and 5% quantile.

		Distal WEPL difference (mm)									
Proton beam angle		**0°**	**20°**	**40°**	**60°**	**80°**	**100°**	**120°**	**140°**	**160°**	**180°**
Patient1	Median	3.7	4.3	4.7	4.7	4.7	5.0	5.5	4.6	2.8	2.1
	95% quantile	13.8	11.2	9.4	8.3	8.5	10.1	15.0	19.2	15.7	11.2
	5% quantile	−7.4	−4.3	−1.0	0.4	1.0	1.2	0.7	−0.6	−2.8	−2.9
Patient2	Median	2.8	2.3	2.5	2.6	2.6	2.6	2.6	2.2	3.3	4.2
	95% quantile	14.7	11.5	9.2	8.4	8.3	9.1	10.7	9.1	8.7	9.6
	5% quantile	−1.3	−0.6	−0.4	−0.5	−0.9	−1.4	−2.3	−4.0	−4.3	0.0
Patient3	Median	1.4	1.2	1.4	1.5	1.7	1.9	2.1	2.5	4.1	3.4
	95% quantile	10.9	8.3	7.3	6.7	6.6	6.9	7.9	8.9	9.2	7.8
	5% quantile	−6.5	−4.3	−2.3	−1.6	−1.6	−1.8	−2.2	−3.4	0.4	−0.8
Patient4	Median	3.2	1.9	0.7	0.0	−0.5	−0.9	−1.3	−1.2	6.8	4.8
	95% quantile	9.7	7.2	6.0	5.4	5.6	6.4	5.8	15.5	15.5	12.8
	5% quantile	−10.0	−8.3	−6.0	−5.1	−5.2	−5.8	−7.4	−11.9	−2.6	−0.8
Patient5	Median	3.9	3.3	3.2	3.2	3.2	3.1	2.8	2.6	2.9	3.7
	95% quantile	16.4	8.5	8.2	8.3	6.9	6.6	7.8	8.0	9.1	9.7
	5% quantile	−4.2	−0.7	0.4	0.6	0.4	0.0	−0.3	−1.0	−1.2	−2.0
Patient6	Median	4.6	5.5	5.1	4.1	3.3	2.9	2.8	2.8	2.5	−0.4
	95% quantile	18.5	16.7	12.6	9.9	8.5	7.6	7.4	8.1	9.5	10.8
	5% quantile	−3.5	0.7	1.1	0.4	−0.1	−0.4	−0.7	−1.3	−2.7	−4.8
Patient7	Median	4.4	3.3	2.7	2.4	2.3	2.6	2.4	1.5	1.5	2.9
	95% quantile	11.5	10.5	9.4	9.0	9.3	9.8	11.3	10.5	14.5	12.0
	5% quantile	0.3	0.4	−0.4	−1.3	−2.0	−2.7	−3.4	−5.3	−5.4	−2.7
Patient8	Median	1.7	1.3	1.3	1.4	1.8	2.6	4.5	8.1	5.8	2.1
	95% quantile	13.3	13.8	10.0	8.1	7.6	8.0	10.6	17.7	18.0	10.8
	5% quantile	−1.6	−1.2	−1.0	−1.0	−0.9	−0.7	−0.6	1.1	0.5	−2.1
Patient9	Median	4.3	4.4	4.6	4.5	4.6	4.7	5.2	5.4	6.1	5.5
	95% quantile	22.5	17.4	12.3	10.4	10.0	11.0	12.7	16.4	17.4	15.1
	5% quantile	−5.5	−1.7	−0.3	0.0	0.2	0.4	0.5	0.4	1.1	0.1
Patient10	Median	3.7	3.5	3.2	3.0	2.7	1.9	0.0	−1.5	−0.1	0.1
	95% quantile	10.3	6.6	5.4	4.7	4.7	5.3	4.8	5.2	4.4	4.0
	5% quantile	−1.4	−0.5	0.1	0.2	−0.5	−3.0	−4.6	−5.2	−3.6	−3.7
Patient11	Median	3.0	3.1	3.6	4.1	4.3	4.7	5.5	6.2	5.3	4.8
	95% quantile	14.3	19.4	15.0	12.9	12.6	13.2	13.8	17.3	17.2	13.3

	Distal WEPL difference (mm)									
Proton beam angle	**0°**	**20°**	**40°**	**60°**	**80°**	**100°**	**120°**	**140°**	**160°**	**180°**
5% quantile	−1.7	−0.2	−0.1	−0.1	−0.2	−0.5	−0.8	−1.2	−0.7	0.1